Opto-Electronic Advances

ISSN 2096-4579 CN 51-1781/TN

Broadband and continuous wave pumped second-harmonic generation from microfiber coated with layered GaSe crystal

Zhen Hao, Biqiang Jiang, Yuxin Ma, Ruixuan Yi, Xuetao Gan and Jianlin Zhao

Citation: Hao Z, Jiang BQ, Ma YX, Yi RX, Gan XT et al. Broadband and continuous wave pumped second-harmonic generation from microfiber coated with layered GaSe crystal. *Opto-Electron Adv* **6**, 230012(2023).

https://doi.org/10.29026/oea.2023.230012

Received: 1 February 2023; Accepted: 7 May 2023; Published online: 19 June 2023

Opto-Electronic Advances

Article

September 2023, Vol. 6, No. 9

DOI: 10.29026/oea.2023.230012

Broadband and continuous wave pumped second-harmonic generation from microfiber coated with layered GaSe crystal

Zhen Hao, Biqiang Jiang*, Yuxin Ma, Ruixuan Yi, Xuetao Gan* and Jianlin Zhao

The conversion-efficiency for second-harmonic (SH) in optical fibers is significantly limited by extremely weak second-order nonlinearity of fused silica, and pulse pump lasers with high peak power are widely employed. Here, we propose a simple strategy to efficiently realize the broadband and continuous wave (CW) pumped SH, by transferring a crystalline GaSe coating onto a microfiber with phase-matching diameter. In the experiment, high efficiency up to 0.08 %$W^{-1}mm^{-1}$ is reached for a C-band pump laser. The high enough efficiency not only guarantees SH at a single frequency pumped by a CW laser, but also multi-frequencies mixing supported by three CW light sources. Moreover, broadband SH spectrum is also achieved under the pump of a superluminescent light-emitting diode source with a 79.3 nm bandwidth. The proposed scheme provides a beneficial method to the enhancement of various nonlinear parameter processes, development of quasi-monochromatic or broadband CW light sources at new wavelength regions.

Keywords: nonlinear optics; second-harmonic generation; continuous wave pump; high efficiency; multi-frequencies mixing; broad spectra; microfibers; gallium selenide

Hao Z, Jiang BQ, Ma YX, Yi RX, Gan XT et al. Broadband and continuous wave pumped second-harmonic generation from microfiber coated with layered GaSe crystal. *Opto-Electron Adv* **6**, 230012 (2023).

Introduction

Optical nonlinear frequency conversion in parametric processes includes harmonic generations, parameter oscillation and four-wave mixing has been widely applied to generate coherent light sources at new wavelengths, or with broadband spectrum, and to amplify weak signals[1–9]. However, due to the centrosymmetry of fused silica fiber, only quite weak surface second-harmonic (SH) can be detected from the pristine optical fibers[10,11]. In optical fibers without integrated nonlinear materials, it is usual to facilitate intrinsic harmonics generation under the pump of pulse lasers with watt-level peak power in structures including fiber loops[12], photonic crystal fibers[13–15], and periodically poled fibers[16–18]. However, as an inherent resonance nature introduced by whispering-gallery mode, narrow operation bandwidths of fiber loop devices will significantly weaken the extensibility of wavelength modulation, and thus greatly limit broadband applications. It is the same case in periodically poled fibers, where the unchanged poled period leads to the operation of only a narrow bandwidth determined by

Key Laboratory of Light Field Manipulation and Information Acquisition, Ministry of Industry and Information Technology, and Shaanxi Key Laboratory of Optical Information Technology, School of Physical Science and Technology, Northwestern Polytechnical University, Xi'an 710129, China.

*Correspondence: BQ Jiang, E-mail: bqjiang@nwpu.edu.cn; XT Gan, E-mail: xuetaogan@nwpu.edu.cn

Received: 1 February 2023; Accepted: 7 May 2023; Published online: 19 June 2023

the quasi-phase matching[19]. Therefore, it is still a challenge to efficiently produce SH signal in a broad wavelength range under a continuous wave (CW) pump, which hinders the development of nonlinear parametric processes in various fields such as new wavelength light sources[20,21], high-resolution microscope imaging[22], and signal processing[23].

In this work, we report the achievement of narrowband/broadband CW-pumped SH in a microfiber assisted by the layered gallium selenide (GaSe) crystal. For an amorphous microfiber[11], by tailoring the waveguide chromatic dispersion in the fabrication process, material dispersion is compensated with mode dispersion[24,25], which makes the phase-matching approximately satisfied for SH. Due to ultrahigh second-order nonlinearity and long-range order structure of the crystalline GaSe, and a large nonlinear interaction length, a bright green SH at 532 nm can be observed with naked eyes. In the popular C-band near 1550 nm, pumped by a picosecond laser, the normalized SH conversion-efficiency per unit length is enhanced by at least 2 orders of magnitude compared with previous schemes implemented with different optical fibers[3,14,24,26–32]. More importantly, the high conversion-efficiency guarantees the CW laser source pumped SH at 775 nm, and this frequency conversion process can be extended to more than one signal wavelengths by mixing multiple frequencies of CW pumps. Moreover, broadband SH spectrum is also achieved under the pump of a CW superluminescent light-emitting diode (SLED) source with a 79.3 nm bandwidth. Therefore, the proposed scheme, opens up a new avenue to efficient and broadband CW-pumped harmonic generation, and can optimize nonlinear processes in optical fibers for extending applications spanning from new wavelength light sources to signal processing.

Device fabrication and characterizations

Figure 1(a) schematically depicts the layered-GaSe coated microfiber for SH excitation and crystal structure of ε-GaSe used in experiments. The microfiber was fabricated, by the flame drawing technique, with a diameter of approximately 3.3 μm in the tapered region, which is close to the optimal diameter for the phase-matched $HE_{11}(\omega)$ and $HE_{31}(2\omega)$, $EH_{11}(2\omega)$ modes[24,27]. The difference between effective refractive indices of $HE_{31}(2\omega)$ and $EH_{11}(2\omega)$ is on the magnitude of 10^{-4}, and the two modes degenerate into the same scalar mode. Their modal distributions are shown in insets of Fig. 1(a). The employed ε-GaSe, with D_{3h} point group with a bilayer stacking order, has a relatively high second-order nonlinear susceptibility[33–36]. With the aid of chemical-free transfer method described in supplemental information and many times' attempts, a relatively complete layered GaSe crystal was transferred on the tapered region of the microfiber. Due to possibly introduced slight mechanical damage to the microfiber, it is necessary to deal with the GaSe-transferred microfiber carefully in following experiments. The optical microscope image of the device is displayed in Fig. 1(b), exhibiting the quite smooth GaSe coating with the length of ~40 μm. As shown in Fig. 1(c), when a source emitting red light at 650 nm was launched into the microfiber, we could see the scattering red light from the GaSe layer under the dark field. The transmission loss of the GaSe-transferred microfiber is measured as approximately 60% at pump wavelength of 1550 nm, and the loss caused independently by the GaSe coating itself can be estimated as 54% due to the >90% transmission of the pristine microfiber.

As an important physical quantity to show the surface morphology, the thickness of the GaSe coating is carefully investigated by an atomic force microscope (AFM). *In-situ* characterization at the boundary of GaSe coating on the microfiber is illustrated in Fig. 1(d) and 1(e). Attributed to the stripping of layered GaSe in the transition process companied by external mechanical stress, more than a single thickness (~72 nm and ~50 nm) was identified, revealing that the GaSe coating consists of two parts. As shown in Fig. 1(f), the Raman spectrum acquired from a GaSe sample adhering on a silicon substrate shows three main peaks at 134.2, 214.0 and 308.6 cm^{-1}. These peaks correspond to the A_{1g}^1, E_{2g}^1 and A_{1g}^2 vibrational modes of crystalline GaSe, verifying its bulk nature determined in Fig. 1(d) and 1(e). However, the information already acquired is still insufficient to uniquely determine coverage ratios of two parts on the microfiber surface, and therefore we further investigated the polarization dependent SH experimentally and theoretically. In the experiment, pumped by a 1550 nm linearly polarized laser (pulse width: 7.6 ps, repetition rate: 18.5 MHz) with adjustable polarization direction, the polarization dependent SH was measured. As depicted in Fig. 1(g), at an interval of 180°, two main maximums appear at 155° and 335°. Additionally, two slightly lower sub-maximums were also observed at 75° and 255°, and this implies that the GaSe coating is a combination of two parts with different thicknesses, which agrees well

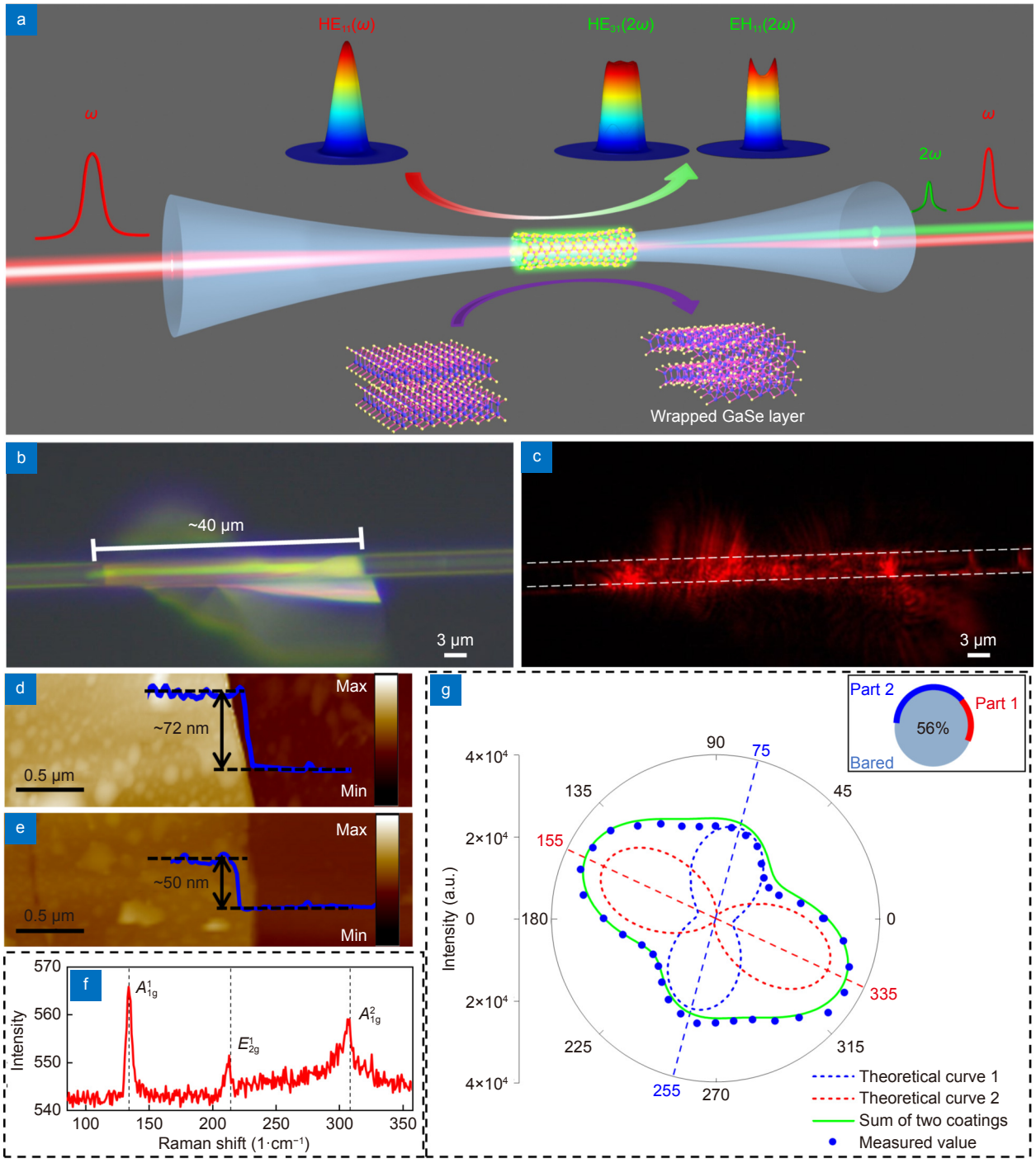

Fig. 1 | Schematic diagram of a microfiber and surface morphologies of the GaSe-transferred microfiber. (**a**) Schematic of the microfiber for exciting SH, with the crystal structure and phase matched modes shown in the inset. (**b**) Optical microscope image of the GaSe-transferred microfiber under bright field, with the scattering light from the GaSe coating shown in (**c**). (**d**, **e**) *In-situ* AFM images of the GaSe layer on the microfiber, with two different thicknesses (72 and 50 nm) found. (**f**) Raman spectrum of the used GaSe layer recorded with 532 nm light, with A_{1g}^1, E_{2g}^1 and A_{1g}^2 vibrational modes identified. (**g**) Measured polarization-dependent SH signal, fitted by the theoretically calculated SH under the 56% equivalent coverage ratio. SH, second-harmonic; AFM, atomic force microscope.

with the characterization results in Fig. 1(d) and 1(e). The polarization dependent SH in Fig. 1(g) fundamentally originated from the quartic relationship between SH intensity and projection of pump electric field on the surface of the GaSe coating (Please see the Supplemental information for details), and formally reflects the relative distribution pattern and coverage ratios of two parts of the GaSe coating. To quantitatively retrieve coverage

ratios of two parts, respective polarization dependences were theoretically calculated, as marked by red and blue dashed curves in Fig. 1(g). The red curve represents the theoretical polarization dependence when Part 1 exists alone, and the blue curve indicates the similar meaning. According to the calculation results, Part 1 and Part 2 (Refer to the inset at top right corner of Fig. 1(g)) account for 22% and 34% of the surface of the microfiber, respectively, indicating an equivalent overall coverage ratio of 56%. Considering that only the cross section of the microfiber is examined, the calculated equivalent coverage ratio is approximately 56% based on the assumption of longitudinal uniformity of the GaSe coating. Moreover, the non-circular symmetry of the GaSe coating may slightly distort transversal electric field distribution of pump and SH modes, which would be alleviated if the microfiber is wrapped by a GaSe coating with a higher coverage ratio.

Results and discussion

When a pump laser is applied to excite SH, considering accumulated SH from different axial positions of the microfiber, the power of output signal ($P_{2\omega}$) is determined by[27,29,30,37,38]

$$P_{2\omega} = P_{\omega}^{2}|\kappa|^{2}L^{2}\mathrm{sinc}^{2}\left(\frac{\Delta\beta_{\mathrm{SH}}L}{2}\right), \tag{1}$$

$$\kappa = \frac{\omega_0\varepsilon_0}{4N_{\omega}\sqrt{N_{2\omega}}}\int\sum_{jkl}\chi_{jkl}^{(2)}\mathrm{e}_{2\omega}^{*j}\mathrm{e}_{\omega}^{k}\mathrm{e}_{\omega}^{l}\mathrm{d}A, \tag{2}$$

$$N_i = \frac{1}{2}\left|\int \boldsymbol{e}_i\times\boldsymbol{h}_i^{*}\cdot\hat{\boldsymbol{z}}\mathrm{d}A\right|, \quad i=1,2, \tag{3}$$

where, L is the nonlinear interaction length, and $\Delta\beta_{\mathrm{SH}}=2\beta_{\omega}-\beta_{2\omega}$ is the phase-mismatch parameter between the pump and SH signal, where β_{ω} and $\beta_{2\omega}$ give their propagation constants, respectively. The nonlinear coupling parameter κ is determined by the coupling of second-order nonlinear polarization to $\mathrm{HE}_{31}(2\omega)$ or $\mathrm{EH}_{11}(2\omega)$ mode, in which e_{ω}^{j} and $\mathrm{e}_{2\omega}^{j}$ express the normalized electric field component of pump and signal mode along j axis (j=x', y', z'). $\chi_{jkl}^{(2)}$ is the tensor element of the second-order nonlinearity, possessing the nonzero elements $\chi_{y'y'y'}^{(2)}=-\chi_{y'x'x'}^{(2)}=-\chi_{x'x'y'}^{(2)}=-\chi_{x'y'x'}^{(2)}$ when x' and y' axes are assigned to zigzag- and armchair direction of GaSe lattice structure[33]. Note that the integration in Eq. (2) is performed in the infinite plane perpendicular to the longitudinal direction of the microfiber. N_1 and N_2 in Eq. (3) represent normalization factors for pump and SH modes, respectively.

The experimental setup for exciting and measuring SH is illustrated in Fig. 2. The pump fundamental waves, provided by linearly polarized near-infrared fiber lasers, were coupled into the single-mode fiber (SMF) through a coarse wavelength division multiplexer (CWDM) and

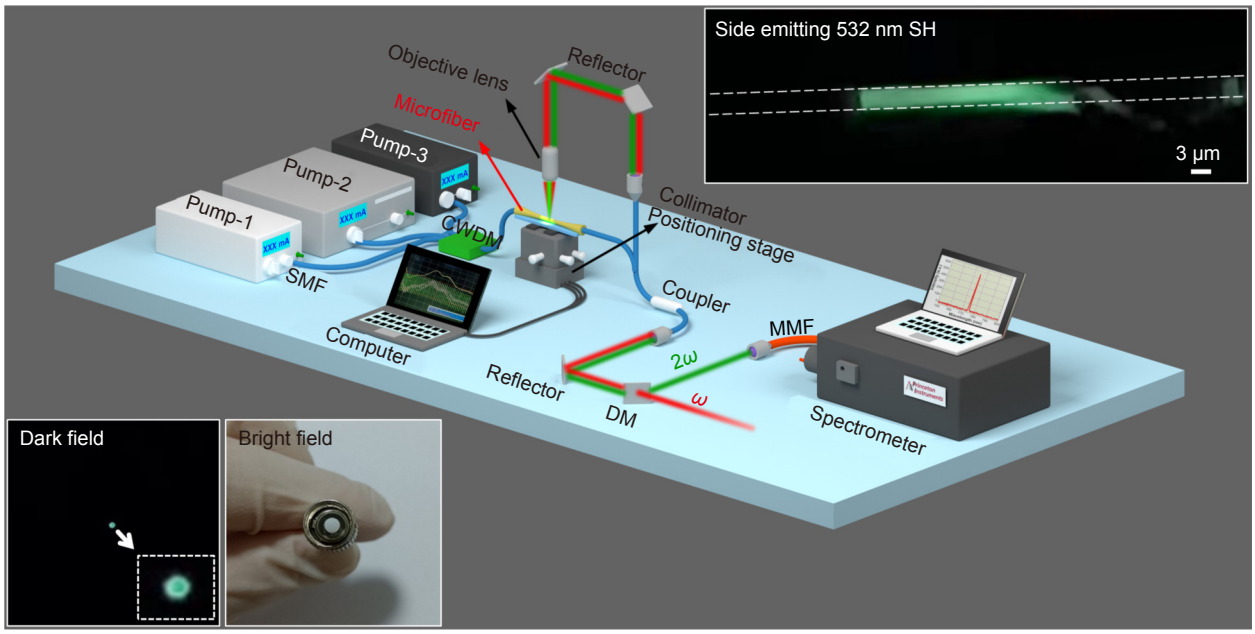

Fig. 2 | Experimental setup for exciting and measuring harmonics. 532 nm SH emitted from the microfiber surface and the end face of the fiber are illustrated in the top and bottom insets, respectively. SH, second-harmonic; SMF, single-mode fiber; MMF, multi-mode fiber; DM, dichroic mirror; CWDM, coarse wavelength division multiplexer.

then intensely interacted with the GaSe coating transferred on the microfiber. Additionally, in order to measure the evolution of the SH along the microfiber axis, a positioning stage and a microscopic objective are installed below and above the microfiber. Finally, in order to separate the produced SH from the pump light, a collimating and filtering system consisting of two collimators (central operation wavelength: 780 nm), a dichroic mirror (long pass: 950 nm) and a reflector (coated with aluminum film) was configured to filter out the pump light. The SH intensity was monitored in real-time by a spectrometer.

To check the quality of the fabricated device in an intuitive way, the GaSe-transferred microfiber was first tentatively pumped by a 1064 nm picosecond laser, with a pulsed width of 11 ps and a repetition rate of 19.5 MHz. When an approximately 80 mW pump laser is incident into the microfiber, by using the experimental setup illustrated in Fig. 2, a distinct side emitting green frequency-doubled light could be observed from the microfiber's surface with naked eyes (Refer to the inset of Fig. 2). Moreover, the rest of green SH at 532 nm coupled into the microfiber and propagated steadily in subsequent fibers. By comparing the two images captured under bright and dark fields, respectively, a small green-spot was identified at the end face of the optical fiber. The zoomed green-spot is shown in the inset of Fig. 2, whose average power was measured as more than 1 μW with a power meter. Therefore, obvious green SH signals emitted from surface and the end face of the fiber prove the high-quality of GaSe-transferred microfiber, which provides great convenience for subsequent experiments implemented with C band pump lasers.

In order to examine the device performance of GaSe-transferred microfiber in the well-required C telecom band, the 1550 nm pulse light was incident into the GaSe-transferred microfiber from the picosecond laser used in the aforementioned polarization dependence experiment. For clear illustration, the SH and third-harmonic (TH) spectra under 0.868 mW were measured

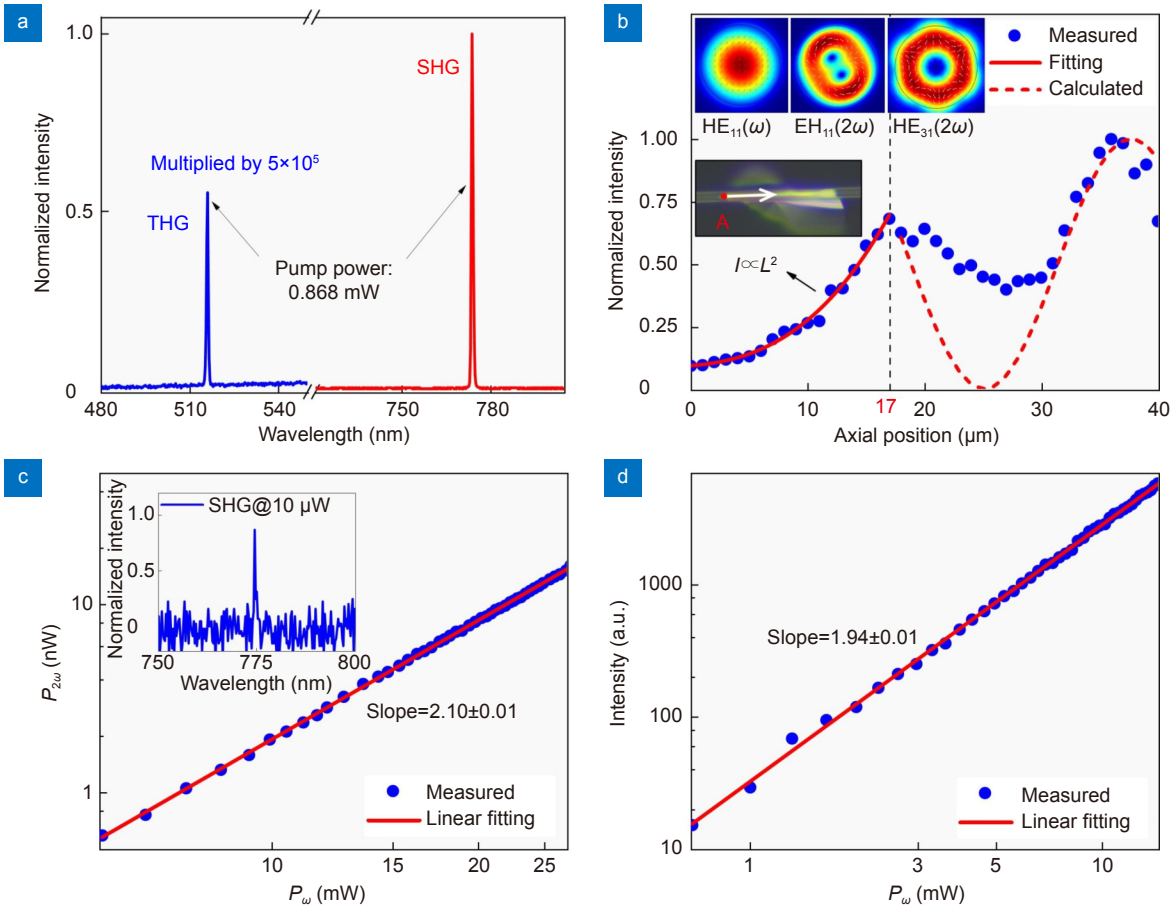

Fig. 3 | (**a**) Spectra of SH at 775 nm and TH at 516.3 nm, pumped by a 0.868 mW picosecond laser. (**b**) Collected local SH intensity along the axial position of microfiber surface. (**c**) Power-dependence of SH pumped by the 1550 nm picosecond laser. (**d**) Power-dependence of SH when pump average power of the CW laser is tuned from 0.7 to 14.5 mW. SH, second-harmonic; TH, third harmonic; CW, continuous-wave.

and plotted in Fig. 3(a). With the assistance of crystalline GaSe layer, the SH and TH intensities have been greatly enhanced, compared with the intrinsic nonlinear signal from the microfiber. As a result, a detectable SH signal can be observed with very weak pump power. Meanwhile, the diameter (~3.3 μm) of the fabricated microfiber is almost the optimal one for the phase matching. According to Eq. (1), the SH signal will be a quadratic trend ($P_{2\omega} \propto L^2$) along the propagation direction in the GaSe coating. To confirm this, we carried out experiments to demonstrate the cumulative result of SH signal along the GaSe-transferred microfiber. The side emitting SH from the GaSe-transferred microfiber was collected using the experimental setup shown in Fig. 2. Starting from the point A shown in the inset of Fig. 3(b) along the positive direction marked with the white arrow, the SH intensity evolves as a quadratic trend when the nonlinear interaction length (or axial coordinate) is less than 17 μm. This quadratic trend supports that approximate phase matching is satisfied between $HE_{11}(\omega)$ and $HE_{31}(2\omega)$, $EH_{11}(2\omega)$, with their transverse mode profiles shown in insets of Fig. 3(b). Due to gradually accumulated phase-mismatching of pump and SH signal, the SH intensity no longer quadratically increased with nonlinear interaction length when axial distance exceeds 17 μm, and the periodic change is calculated under a phase-mismatching parameter of 0.25 rad/μm, as depicted by the red dashed line in Fig. 3(b). Specially, due to the relatively high refractive index (~2.8) of GaSe for the pump and SH, the GaSe layer will introduce the accumulated phase mismatching. And then, the produced SH signal would be weakened especially for a large nonlinear interaction length, and thus there is an optimal coating length.

By increasing the incident average power from 5.6 to 27.3 mW, the SH power increased quadratically with a fitting slope of 2.10±0.01, as shown in Fig. 3(c), which was in real-time monitored by a high-precision power meter (Thorlabs, PM320E) instead of the spectrometer. It is notable that the measured maximum average power of SH was up to approximately 16 nW, corresponding to a normalized frequency conversion-efficiency of 0.08 $\%W^{-1}mm^{-1}$ on the unit nonlinear interaction length (The average power of SH and pump light is used in the calculation of conversion-efficiency). The efficiency is at least 2 orders of magnitude higher than most previously reported experiments conducted with other optical fibers[3,14,24,26–32], as listed in Table 1. Provided that the pulse width and repetition rate of SH signal are the same as that of pump laser (7.6 ps, 18.5 MHz), abovementioned 16 nW average power of SH corresponds to approximately 0.1 mW peak power. Subsequently, the pump average power was reduced to 10 μW, but SH signal in the inset of Fig. 3(c) still remained detectable by the spectrometer, demonstrating the microwatt-level excitation threshold. Considering the high conversion-efficiency, we replaced the pulse laser with a 1550 nm CW laser to excite the SH. According to the intensity evolution of SH signal shown in Fig. 3(d), CW-pumped SH

Table 1 | Comparison of SH efficiency or enhancement in different fibers.

Fiber type	Integrated material	Integration method	Interaction length [mm]	Pump wavelength [nm]	Pump duration	Efficiency or enhancement	ref.
Photonic crystal fiber	Xe	Filled	160	1064	2 ns	5×10^{-11} $\%W^{-1}mm^{-1}$	ref.[26]
Photonic crystal fiber	None	None	150	820	120 fs	2.1×10^{-6} $\%W^{-1}mm^{-1}$	ref.[14]
Doped fiber	S/Te hybrid	Doped	25	1800	200 fs	1.1×10^{-7} $\%W^{-1}mm^{-1}$	ref.[31]
Suspended-core fiber	GaSe	Filled	0.56	1550	8.8 ps	4.2×10^{-7} $\%W^{-1}mm^{-1}$	ref.[28]
Birefringent fiber	None	None	230	1550	CW	8.7×10^{-5} $\%W^{-1}mm^{-1}$	ref.[32]
Hollow-core fiber	GaSe	Filled	0.36	1550	8.8 ps	1.5×10^{-8} $\%W^{-1}mm^{-1}$	ref.[30]
Hollow-core fiber	MoS_2	Grown	250	1800	150 fs	4×10^{-4} $\%W^{-1}mm^{-1}$	ref.[3]
Microfiber	WS_2	Transferred	0.06	1550	10 ns	333 times mm^{-1} [a]	ref.[29]
Microfiber	InSe	Deposited	2	1550	CW	1.7×10^{-11} $\%W^{-1}mm^{-1}$	ref.[27]
Microfiber	GaSe	Deposited	4	1550	10 ps or CW	4×10^{-6} $\%W^{-1}mm^{-1}$	ref.[24]
Microfiber	GaSe	Transferred	0.04	1550	7.6 ps or CW	0.08 $\%W^{-1}mm^{-1}$	This work

[a] Compared with SH excited in a pristine microfiber.

scales quadratically with excitation power from 0.7 to 14.5 mW with a fitting slope of 1.94±0.01. Compared with the excitation power of 1 mW under CW pump in the previous report[24], the threshold of producing detectable SH in GaSe-transferred microfiber has been reduced to approximately 0.7 mW. It is important to note that, whatever the high conversion-efficiency pumped by a picosecond laser or the low threshold power pumped by a CW laser, these can be attributed to the ultrahigh second-order nonlinearity, large nonlinear interaction length and especially the long-range order structure of the crystalline GaSe. Compared with randomly distributed GaSe nanosheets, the long-range order structure of the GaSe crystal ensures the homogeneous constructive interference of SH excited at different axial positions, promoting the approximately two orders of magnitude's enhancement of SH.

Further, CW pumped frequency conversion process supplied by a single laser source can be extended to more than one signal wavelengths by mixing multiple frequencies of pump light. As an example, three CW tunable lasers (TL) within O/C/L bands (1270/1550/1590 nm for TL_1/TL_2/TL_3) were coupled together through a coarse wavelength division multiplexer (CWDM) shown in Fig. 2 to implement the multi-frequencies conversion process. The corresponding typical spectrum is shown in Fig. 4(a), when the pump power of TL_1/TL_2/TL_3 is fixed at 10/15/10 mW separately. It should be noted that the total number of SH and SF equals to $n+C_n^2=n(n+1)/2$, where n is the number of pump wavelengths and also SH signals. C_n^2 represents the number of combinations when two of the n pump wavelengths are selected, namely the number of sum-frequency (SF) signals. In the experiment, n=3 leads to overall six observable frequency conversion signals, in which three SH signals for $2\omega_1$/$2\omega_2$/$2\omega_3$ at 635/775/795 nm and three SF signals for $\omega_1+\omega_2$, $\omega_1+\omega_3$ and $\omega_2+\omega_3$ at 698.05, 706.05 and 784.87 nm (Please see the Supplemental information for inherent distribution pattern of SH and SF peaks in the frequency region). Moreover, we investigated the power dependence of six frequency conversion signals on the power of TL_1, by changing its power from 0 to 10 mW. From the evolution shown in Fig. 4(b), we can observe three gradually grown SH ($2\omega_1$) and SF signals ($\omega_1+\omega_2$, $\omega_1+\omega_3$) with the pump power, while intensities of the rest three frequency conversion signals remain almost unchanged. Corresponding slopes of power dependences for $2\omega_1$, $\omega_1+\omega_2$, $\omega_1+\omega_3$ are 1.95±0.03, 0.97±0.01 and 0.99±0.01, respectively. Subsequently, similar power dependence characteristics were investigated by changing pump power of TL_2 and TL_3, respectively, with their evolutions illustrated in Fig. 4(d, f). The three increased signal intensities of $2\omega_2$, $\omega_1+\omega_2$, $\omega_2+\omega_3$ (Or $2\omega_3$, $\omega_1+\omega_3$, $\omega_2+\omega_3$) under pump of TL_2 (TL_3) present log-log plotted slopes of 1.92±0.01 / 0.98±0.01 / 1.05±0.01 (1.99±0.01 / 1.00±0.01 / 0.99±0.01), as shown in Fig. 4(e) and Fig. 4(g). These good agreements with theoretical predictions prove that the proposed device operates as an excellent platform for multi-frequencies conversion.

Achieving broadband SH with high efficiency is a significant challenge regardless of whether the experimental scheme is free-space with bulky material or a compact device of optical fiber. However, in the proposed fully integrated micro-nano optics platform, a superluminescent light-emitting diode (SLED) source with a broadband optical spectrum and low power spectral intensity, was used to achieve a broadband SH in the GaSe-transferred microfiber (Similar experimental results implemented by an amplified spontaneous emission (ASE) source is given in the Supplemental information). From spectral evolution in Fig. 5(a), we can observe a gradually grown broadband SH that is centered around 773 nm, when the pump power is changed from 1.8 to 13.9 mW. By extracting maximum intensity of each spectrum, the slope of power dependence is calculated as 2.01±0.02, which agrees well with theoretical value 2, as shown in Fig. 5(b). Then, we compared the Gaussian-shaped spectrum of broadband SH with that of SLED source, as shown in Fig. 5(c). According to the top subplot in Fig. 5(c), the smooth spectrum of the SLED source covers the whole C-band, possessing a 79.3 nm full width at −10 dB maximum (1514.5~1593.8 nm). In contrast, the produced SH continuum spans from 761.9 to 790.2 nm, revealing a 28.3 nm bandwidth. This bandwidth is a relatively large one compared with previous reports[3,14,24,26–32], demonstrating the excellent operation performance of the GaSe-transferred microfiber. The more than half reduced bandwidth with respect to the SLED spectrum is attributed to the frequency double process, and the ratio between SH and pump bandwidths is 0.357, which is very close to the theoretical value of 0.354 (Please see the Supplemental information for the details of derivation). Note that the theoretical ratio between SH and pump bandwidths is determined by the specific profile of pump spectrum. Compared with broadened SH ensured by self-phase modulation and cross-phase modulation[39], a broadband frequency-double signal can be produced in a

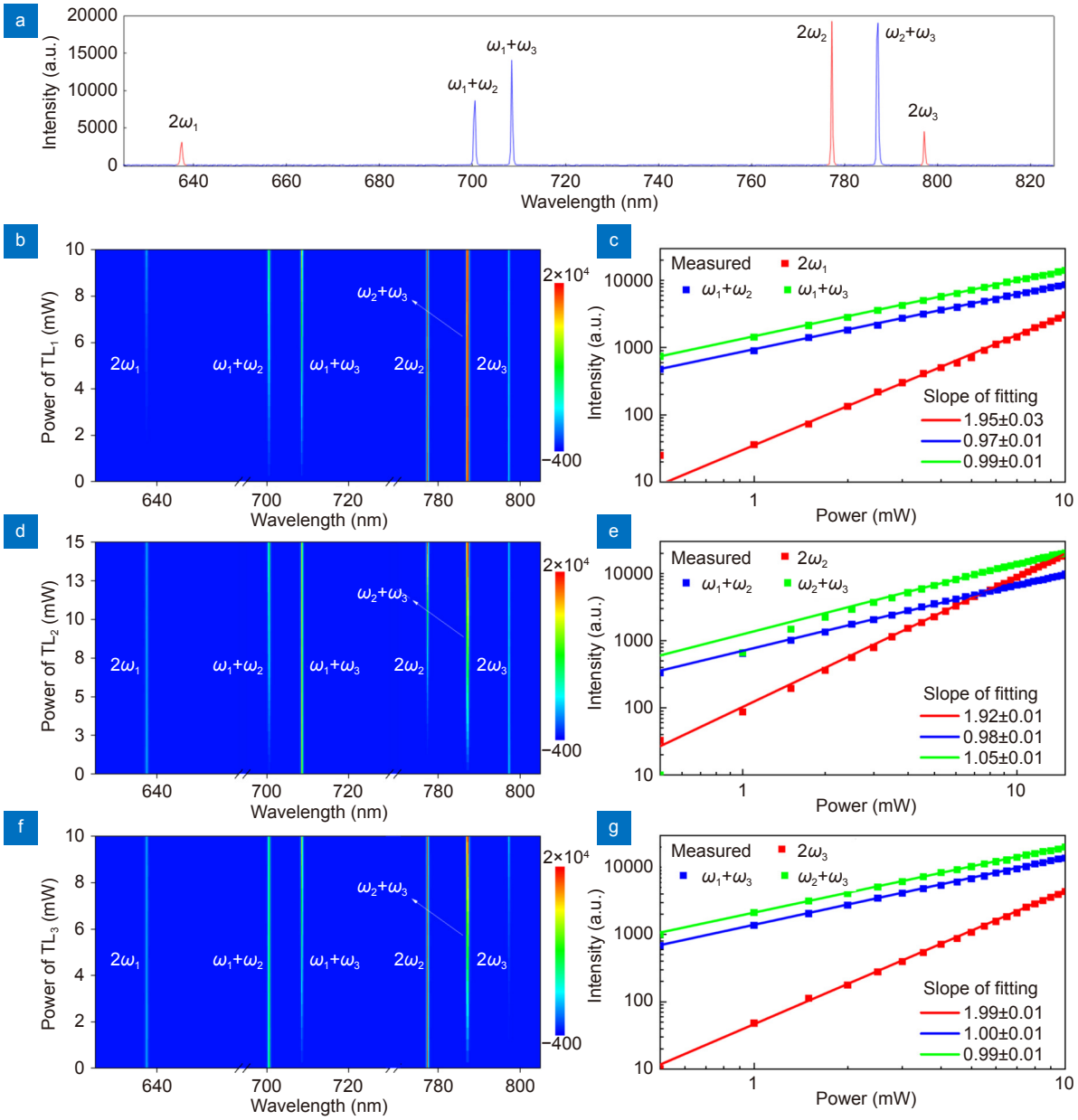

Fig. 4 | (**a**) Typical spectrum of SH and SF at six frequency conversion wavelengths (SH: 635/775/795 nm, SF: 698.05/706.05/784.87 nm), pumped by three CW lasers at 1270/1550/1590 nm simultaneously. (**b**) Intensity evolution when pump power of TL_1 is varied from 0 to 10 mW. (**c**) Log-log plotted intensities of three frequency conversion signals (SH: 635 nm, SF: 698.05/706.05 nm) that increased with the pump power of 1270 nm laser. Similar power dependences were investigated by changing pump power of TL_2 and TL_3 respectively, with their evolutions and log-log plotted slopes illustrated in Fig. 4(d–g). SH, second-harmonic; SF, sum-frequency; CW, continuous wave; TL, tunable laser.

simpler way in our scheme without utilizing third-order nonlinearity of the device itself. The additional merit of the scheme is that the modulation of spectrum intensity can be fulfilled simply by varying the injected pump power rather than modulating the reverse-biased voltage in a silicon waveguide, which is considered as a reliable method intuitively.

To evaluate the nonlinear conversion performance, the detailed comparisons are given based on schemes listed in Table 1. In the scheme with photonic crystal fibers[14,26], the SH signal is detected to follow a sinc^2 dependence on the Xe gas pressure, with a conversion-efficiency of 5×10^{-11} $\%W^{-1}mm^{-1}$. By functionalizing the hollow-core fiber with molybdenum-disulfide (MoS_2) or GaSe nanosheets[3,30], the SH signal is enhanced to three orders of magnitude that of monolayered MoS_2, with a conversion-efficiency of 4×10^{-4} $\%W^{-1}mm^{-1}$. The SH signal can also be enhanced in special optical fibers such as the doped fiber[31], suspended-core fiber[28], and birefringent fiber[32]. Widely tunable SH is produced in the range

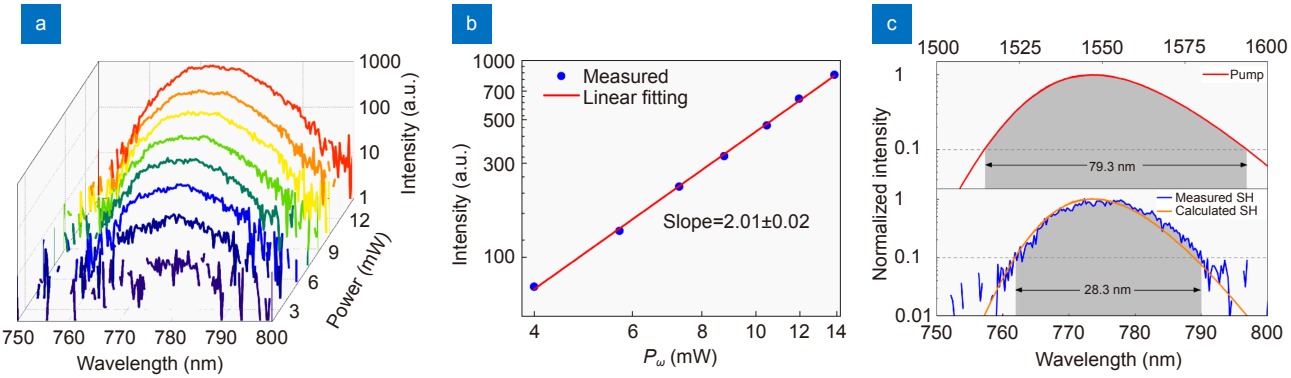

Fig. 5 | (**a**) Spectral evolution of broadband SH centering around 773 nm when the pump power of SLED source is varied from 1.8 to 13.9 mW, and corresponding power dependence is log-log plotted in (**b**). (**c**) The comparison of spectral widths between SH continuum and corresponding pump source of 7.3 mW. SH, second-harmonic; SLED, Superluminescent light-emitting diode.

of 850 to 1502 nm with a conversion-efficiency of 1.1×10^{-7} %W^{-1}mm^{-1}. However, the photonic bandgap effect or large propagation losses of guided modes in above schemes hinder the efficient and broadband SH excitation. Recently, the conversion-efficiency could be further enhanced by coating the monolayer tungsten-disulfide (WS_2), layered GaSe or indium-selenide (InSe) nanosheets on microfibers[24,27,29]. In our proposed scheme, the layered GaSe crystal with a long-range ordered structure was wrapped around the microfiber. Such a device with a short nonlinear interaction length (only several tens of micrometers), can not only obtain the CW-pumped narrowband SH, but also the broadband (28.3 nm) SH continuum pumped by a SLED source with low power spectral density and multi-frequencies mixing processes supported by three CW light sources. The proposed scheme therefore provides a new strategy to construct compact in-fiber or on-chip photonic devices for optical nonlinear processes.

Conclusions

In summary, we report an accessible strategy to efficiently realize the narrowband/broadband CW-pumped SH in a GaSe-transferred microfiber. Benefitting from the ultrahigh second-order nonlinearity and the long-range order structure of transferred GaSe coating, 532 nm green SH signal at the microwatt level can be observed with naked eyes. As expected, under the C-band picosecond pulse pump of 1550 nm, quite high frequency conversion-efficiency up to 0.08 %W^{-1}mm^{-1} has been realized. The conversion-efficiency is enhanced by at least 2 orders of magnitude in comparison with previous reports implemented with other fibers[3,14,24,26–32]. Then, by replacing the pump as a 1550 nm CW laser, we demonstrate CW pumped quasi-monochromatic SH signal at 775 nm. Furthermore, six SH and SF signals at different wavelengths are achieved under the simultaneous pump of three CW lasers. Consequently, the well-established CW operation brings about SLED pumped broadband SH with a bandwidth up to 28.3 nm. By applying chemical vapor deposition method to grow a few atomic layers of nonlinear crystals onto the microfiber[3,15,40], it is promising to the scalable fabrication of the proposed frequency-conversion device. Therefore, we believe that this work is important not only for the enhancement of nonlinear parametric processes in fiber optics, but also for advancing various CW and broadband light sources at new wavelength regions.

References

1. Franken PA, Hill AE, Peters CW, Weinreich G. Generation of optical harmonics. *Phys Rev Lett* **7**, 118–119 (1961).
2. Carman RL, Chiao RY, Kelley PL. Observation of degenerate stimulated four-photon interaction and four-wave parametric amplification. *Phys Rev Lett* **17**, 1281–1283 (1966).
3. Zuo YG, Yu WT, Liu C, Cheng X, Qiao RX et al. Optical fibres with embedded two-dimensional materials for ultrahigh nonlinearity. *Nat Nanotechnol* **15**, 987–991 (2020).
4. Wang BB, Ji YF, Gu LP, Fang L, Gan XT et al. High-efficiency second-harmonic and sum-frequency generation in a silicon nitride microring integrated with few-layer GaSe. *ACS Photonics* **9**, 1671–1678 (2022).
5. Zhu ML, Zhong MZ, Guo X, Wang YS, Chen ZH et al. Efficient and anisotropic second harmonic generation in few-layer SnS film. *Adv Opt Mater* **9**, 2101200 (2021).
6. Krause B, Mishra D, Chen JY, Argyropoulos C, Hoang T. Nonlinear strong coupling by second-harmonic generation enhancement in plasmonic nanopatch antennas. *Adv Opt Mater* **10**, 2200510 (2022).
7. Hao Z, Jiang BQ, Ma YX, Yi RX, Jin HY et al. Strain-controlled phase matching of optical harmonic generation in microfibers. *Phys Rev Appl* **19**, L031002 (2023).
8. Ren J, Lin H, Zheng XR, Lei WW, Liu D et al. Giant and light modifiable third-order optical nonlinearity in a free-standing

h-BN film. *Opto-Electron Sci* **1**, 210013 (2022).
9. Li C L, Liu J C, Zhang F M et al. Review of nonlinearity correction of frequency modulated continuous wave LiDAR measurement technology. *Opto-Electron Eng* **49**, 210438 (2022).
10. Javůrek D, Peřina Jr J. Analytical model of surface second-harmonic generation. *Sci Rep* **9**, 4679 (2019).
11. Fujii Y, Kawasaki BS, Hill KO, Johnson DC. Sum-frequency light generation in optical fibers. *Opt Lett* **5**, 48–50 (1980).
12. Gouveia MA, Lee T, Ismaeel R, Ding M, Broderick NGR et al. Second harmonic generation and enhancement in microfibers and loop resonators. *Appl Phys Lett* **102**, 201120 (2013).
13. Ménard JM, Köttig F, Russell PSJ. Broadband electric-field-induced LP_{01} and LP_{02} second harmonic generation in Xe-filled hollow-core PCF. *Opt Lett* **41**, 3795–3798 (2016).
14. Yuan JH, Sang XZ, Wu Q, Zhou GY, Li F et al. Generation of second-harmonics near ultraviolet wavelengths from femtosecond pump pulses. *IEEE Photon Technol Lett* **28**, 1719–1722 (2016).
15. Chen K, Zhou X, Cheng X, Qiao RX, Cheng Y et al. Graphene photonic crystal fibre with strong and tunable light–matter interaction. *Nat Photonics* **13**, 754–759 (2019).
16. Kashyap R. Phase-matched periodic electric-field-induced second-harmonic generation in optical fibers. *J Opt Soc Am B* **6**, 313–328 (1989).
17. Canagasabey A, Corbari C, Gladyshev AV, Liegeois F, Guillemet S et al. High-average-power second-harmonic generation from periodically poled silica fibers. *Opt Lett* **34**, 2483–2485 (2009).
18. Nasu H, Okamoto H, Kurachi K, Matsuoka J, Kamiya K et al. Second-harmonic generation from electrically poled SiO_2 glasses: effects of OH concentration, defects, and poling conditions. *J Opt Soc Am B* **12**, 644–649 (1995).
19. Boyd RW. *Nonlinear Optics* 3rd ed (Elsevier, Amsterdam, 2008).
20. Yu ZQ, Zhang N, Wang JX, Dai ZJ, Gong C et al. 0.35% THz pulse conversion efficiency achieved by Ti: sapphire femtosecond laser filamentation in argon at 1 kHz repetition rate. *Opto-Electron Adv* **5**, 210065 (2022).
21. Lin XJ, Feng QC, Zhu Y, Ji SH, Xiao B et al. Diode-pumped wavelength-switchable visible Pr^{3+}: YLF laser and vortex laser around 670 nm. *Opto-Electron Adv* **4**, 210006 (2021).
22. Raghunathan V, Han Y, Korth O, Ge NH, Potma EO. Rapid vibrational imaging with sum frequency generation microscopy. *Opt Lett* **36**, 3891–3893 (2011).
23. Liao K, Chen Y, Yu ZC, Hu XY, Wang XY et al. All-optical computing based on convolutional neural networks. *Opto-Electron Adv* **4**, 200060 (2021).
24. Jiang BQ, Hao Z, Ji YF, Hou YG, Yi RX et al. High-efficiency second-order nonlinear processes in an optical microfibre assisted by few-layer GaSe. *Light Sci Appl* **9**, 63 (2020).
25. Agrawal GP. *Nonlinear Fiber Optics* 6th ed (Elsevier, Amsterdam, 2019).
26. Ménard JM, Russell PSJ. Phase-matched electric-field-induced second-harmonic generation in Xe-filled hollow-core photonic crystal fiber. *Opt Lett* **40**, 3679–3682 (2015).
27. Hao Z, Jiang BQ, Hou YG, Li CY, Yi RX et al. Continuous-wave pumped frequency upconversions in an InSe-integrated microfiber. *Opt Lett* **46**, 733–736 (2021).
28. Ma YX, Jiang BQ, Guo YS, Zhang PW, Cheng TL et al. Suspended-core fiber with embedded GaSe nanosheets for second harmonic generation. *Opt Express* **30**, 32438–32446 (2022).
29. Chen JH, Tan J, Wu GX, Zhang XJ, Xu F et al. Tunable and enhanced light emission in hybrid WS_2-optical-fiber-nanowire structures. *Light Sci Appl* **8**, 8 (2019).
30. Hao Z, Ma YX, Jiang BQ, Hou YG, Li AL et al. Second harmonic generation in a hollow-core fiber filled with GaSe nanosheets. *Sci China Inf Sci* **65**, 162403 (2022).
31. Cheng TL, Gao WQ, Kawashima H, Deng DH, Liao MS et al. Widely tunable second-harmonic generation in a chalcogenide-tellurite hybrid optical fiber. *Opt Lett* **39**, 2145–2147 (2014).
32. Zhu EY, Qian L, Helt LG, Liscidini M, Sipe JE et al. Phase-matching with a twist: second-harmonic generation in birefringent periodically poled fibers. *J Opt Soc Am B* **27**, 2410–2415 (2010).
33. Allakhverdiev KR, Yetis MÖ, Özbek S, Baykara TK, Salaev EY. Effective nonlinear GaSe crystal. optical properties and applications. *Laser Phys* **19**, 1092–1104 (2009).
34. Bringuier E, Bourdon A, Piccioli N, Chevy A. Optical second-harmonic generation in lossy media: application to GaSe and InSe. *Phys Rev B* **49**, 16971–16982 (1994).
35. Zhou X, Cheng JX, Zhou YB, Cao T, Hong H et al. Strong second-harmonic generation in atomic layered GaSe. *J Am Chem Soc* **137**, 7994–7997 (2015).
36. Sutherland RL. *Handbook of Nonlinear Optics* 2nd ed (CRC Press, Boca Raton, 2003).
37. Ciret C, Alexander K, Poulvellarie N, Billet M, Arabi CM et al. Influence of longitudinal mode components on second harmonic generation in III-V-on-insulator nanowires. *Opt Express* **28**, 31584–31593 (2020).
38. Lægsgaard J. Theory of surface second-harmonic generation in silica nanowires. *J Opt Soc Am B* **27**, 1317–1324 (2010).
39. Singh N, Raval M, Ruocco A, Watts MR. Broadband 200-nm second-harmonic generation in silicon in the telecom band. *Light Sci Appl* **9**, 17 (2020).
40. Liao F, Yu JX, Gu ZQ, Yang ZY, Hasan T et al. Enhancing monolayer photoluminescence on optical micro/nanofibers for low-threshold lasing. *Sci Adv* **5**, eaax7398 (2019).

Acknowledgements

We are grateful for financial supports from National Natural Science Foundation of China (No. 61975166, 11634010); Key Research and Development Program (No. 2017YFA0303800). We also thank the Analytical & Testing Center of NPU for their assistance with the material and device characterizations.

Author contributions

Z. Hao, B. Q. Jiang and X. T. Gan proposed the original idea. Z. Hao fabricated the sample and performed the measurements, assisted by Y. X. Ma and R. X. Yi. Y. X. Ma and R. X. Yi carried out Raman/AFM characterization of the sample. Z. Hao wrote the original manuscript, revised by B. Q. Jiang, X. T. Gan and J. L. Zhao. B. Q. Jiang, X. T. Gan and J. L. Zhao provided resource support and supervised the project.

Competing interests

The authors declare no competing financial interests.

Supplementary information

Supplementary information for this paper is available at https://doi.org/10.29026/oea.2023.230012